

Mobility and persistence of methane in groundwater in a controlled-release field experiment

Aaron G. Cahill^{1,2}, Colby M. Steelman¹, Olenka Forde², Olukayode Kuloyo³, S. Emil Ruff³, Bernhard Mayer³, K. Ulrich Mayer², Marc Strous³, M. Cathryn Ryan³, John A. Cherry¹ and Beth L. Parker^{1*}

Expansion of shale gas extraction has fuelled global concern about the potential impact of fugitive methane on groundwater and climate. Although methane leakage from wells is well documented, the consequences on groundwater remain sparsely studied and are thought by some to be minor. Here we present the results of a 72-day methane gas injection experiment into a shallow, flat-lying sand aquifer. In our experiment, although a significant fraction of methane vented to the atmosphere, an equal portion remained in the groundwater. We find that methane migration in the aquifer was governed by subtle grain-scale bedding that impeded buoyant free-phase gas flow and led to episodic releases of free-phase gas. The result was lateral migration of gas beyond that expected by groundwater advection alone. Methane persisted in the groundwater zone despite active growth of methanotrophic bacteria, although much of the methane that vented into the vadose zone was oxidized. Our findings demonstrate that even small-volume releases of methane gas can cause extensive and persistent free phase and solute plumes emanating from leaks that are detectable only by contaminant hydrogeology monitoring at high resolution.

Unconventional petroleum development¹ has generated controversy regarding the occurrence, magnitude and effects of fugitive methane leakage^{2,3} from imperfectly sealed well bores^{4,5}. Identifying the frequency, origin and pathways of fugitive methane in the subsurface^{6,7} is paramount to understanding its potential impacts on our fresh groundwater resources. Numerous field techniques have been developed in an attempt to detect methane leakage^{8–10}, while scenario-based numerical modelling has been used to assess subsurface behaviours¹¹. However, no field research has specifically or comprehensively addressed methane migration and fate in the subsurface at high spatiotemporal resolution to more rigorously understand the dominant mechanisms and their interactions. Consequently, evidence-based conceptual understandings of mechanisms controlling fugitive methane distribution in freshwater aquifers remain weak despite expert panel recommendations to examine potential environmental impacts^{12,13}.

Methane leakage from oil and gas wells occurs in an estimated 1–3% of unconventional wells due to imperfect well bore seals^{2,14}. The seals are formed of cement and are geochemically unstable in the saline formations through which the wells are emplaced¹⁵, resulting in eventual deterioration and leakage. However, controversy arises because the typical measurements conducted at well heads consider only gas leaking up along the well casings to the atmosphere¹⁶, and neglect the potential for methane escaping the well casing into geologic formations and migrating within the subsurface, potentially impacting potable groundwater resources. A series of papers that relied only on sampling existing domestic and farm water wells in active shale gas plays in Pennsylvania^{8,17} claim that methane occurrence was common within a kilometre of the well; however, other studies claim this methane is explained

by processes not related to shale gas development^{18–20}. Much of this debate originates from inherent ambiguities in measurements obtained from domestic water wells¹⁹ that are merely receptors of contaminants, as opposed to properly engineered groundwater monitoring networks to understand source–receptor relationships^{19,21}.

Here, we present the results of a multi-disciplinary field experiment that examined the movement, impacts and fate of free-gas methane injected into a shallow freshwater aquifer comprised of nearly homogeneous, Pleistocene beach sand located at CFB Borden, Ontario, Canada, a well-established aquifer research facility (Fig. 1a). We considered surface gas efflux and ground-penetrating radar (GPR) measurements to track subsurface free-gas movement, along with aqueous chemistry (including dissolved gases and C isotope ratios of methane) and microbial characterization to assess the nature and extent of groundwater quality impacts in the well-characterized Borden aquifer^{22,23} under natural conditions of geologic heterogeneity, groundwater flow and hydrochemistry.

Hydrogeologic monitoring construct

Methane ($\sim 51 \text{ m}^3$ or 36.4 kg at standard temperature and pressure) was injected using electronic mass flow control valves simultaneously into two 45° -angled drive-point wells over 72 days at two depths situated at 4.5 and 9 m below ground surface (Fig. 1b). A four-phase injection schedule was used with rates of 0.17, 1.0 and $4.3 \text{ m}^3 \text{ d}^{-1}$ (Supplementary Table 1), which represent the low to medium range in surface casing vent flows observed in Alberta and British Columbia, Canada¹⁴. Monitoring was performed for 245 days after start of injection across a network of depth-discrete monitoring points (Fig. 1b,c). The groundwater monitoring network was designed on the basis of previous Borden aquifer²⁴ and CO_2 gas

¹G360 Institute for Groundwater Research, University of Guelph, Ontario N1G 2W1, Canada. ²Department of Earth, Ocean and Atmospheric Science, University of British Columbia, British Columbia V6T 1Z4, Canada. ³Department of Geoscience, University of Calgary, Calgary, Alberta T2N 1N4, Canada.
*e-mail: bparker@uoguelph.ca

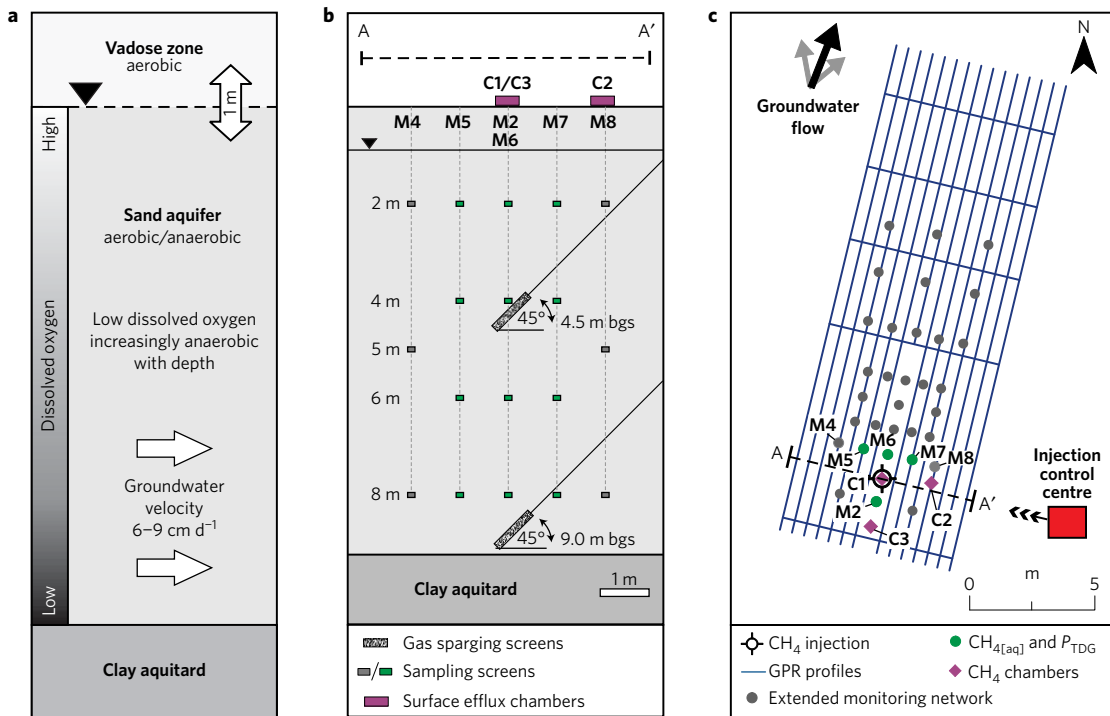


Figure 1 | Hydrologic setting and experimental set-up of the methane injection experiment. **a**, Borden aquifer consisting of a thin vadose zone and a relatively homogeneous sandy aquifer underlain by a clay aquitard. The upper injector is located in the aerobic zone and the lower one in the anaerobic zone where there is slightly higher baseline dissolved methane and increased sulfate. **b**, Cross-section of groundwater monitoring network adjacent to injection points. bgs, below ground surface. **c**, Plan view of monitoring network including multilevel piezometers, surface efflux chambers and geophysical profile lines. The injection control centre consisted of a mobile laboratory, methane canisters and computer-controlled mass flow valves.

injection experiments²⁵. Methane efflux was monitored at surface and within the vadose zone (Fig. 1b,c), while GPR was used to monitor the migration of the gas phase in the aquifer (Fig. 1c).

The aquifer consists of 9 m of horizontal, interconnected lenses ranging from silt to coarse-grained sand with limited heterogeneity, underlain by a silty-clay aquitard. Concentrations of dissolved methane are naturally low (0.02 to 0.2 mg l⁻¹, where 1 mg l⁻¹ of methane equals 0.0027 ccSTP l⁻¹) and baseline methane is biogenic with potential methane oxidation ($\delta^{13}\text{C-CH}_4$ ranges from -80 to $-48\text{\textperthousand}$). The total injected methane has the capacity to impact 2,282.5 m³ of aquifer on the basis of a solubility of 45.6 mg l⁻¹ (Supplementary Information).

Methane migration and fate in the aquifer

Our results show rapid and widespread horizontal migration of free-gas methane along bedding coupled to buoyancy-driven upward migration in the Borden aquifer, resulting in an extensive, continuous, dispersed zone of dissolved methane and hydrochemistry changes (Figs 2–4 and Supplementary Fig. 2). Total dissolved gas pressure (P_{TDG}), which qualitatively indicates the sum of dissolved and free-phase gases in the subsurface²⁶, evolved in an episodic manner (Fig. 2c) with pressure increases preceding build-up of $[\text{CH}_4]_{\text{(aq)}}$ (dissolved methane concentration). $[\text{CH}_4]_{\text{(aq)}}$ increased across all depths after a pause in gas injection (days 39 to 44), and after the injection stopped on day 72 (Fig. 2b), to concentrations that indicate explosion risk following ex-solvation into a confined space ($>10\text{ mg l}^{-1}$ as the accepted lower explosion limit)²⁷. Following resumption of methane injection on day 44, P_{TDG} increased or stabilized while $[\text{CH}_4]_{\text{(aq)}}$ decreased below the explosion risk limit (Fig. 2b,c). This temporary decrease in $[\text{CH}_4]_{\text{(aq)}}$ is potentially a result of displacement of CH_4 -charged water by, or mixing with un-impacted groundwater.

The injection of pressurized gas into a permeable geologic unit typically results in the formation of free-gas migration pathways or

channels²⁸. During gas injection, methane transfer from gaseous to aqueous phase appears limited during periods of free-gas migration or channelling²⁹. Following termination of methane injection, free-gas pressure decreases allow groundwater to re-saturate the pore space and increase surface area for transfer between gas and aqueous phases, resulting in the observed $[\text{CH}_4]_{\text{(aq)}}$ increases (Fig. 2b). While free-gas migration channelling is recognized as limiting subsurface gas retention and efficacy of air-sparging remediation strategies³⁰, its importance in the migration and fate of fugitive methane from energy resource development has not yet been rigorously explored.

The highest concentrations and spatial extent of $[\text{CH}_4]_{\text{(aq)}}$ occurred on day 113 (41 days following termination of gas injection), with concentrations $>25\text{ mg l}^{-1}$ (Supplementary Fig. 1). After 245 days, methane concentrations $>10\text{ mg l}^{-1}$ were observed at 2 and 6 m depths, demonstrating persistence of injected methane (Supplementary Fig. 1). Attenuation of $[\text{CH}_4]_{\text{(aq)}}$ and general water quality impacts were minimal at the time of last sampling, showing slight increases in alkalinity (~ 4.3 to 5.3 meq l^{-1}), decreases in pH (~ 7.3 to 7.0), and consistent increases in cation concentrations, including trace metals (for example, Al, Ni, Sr), directly around (that is, 1 to 2 m distance) the injection zone (Supplementary Table 2). The evolution of pH, alkalinity and aqueous Ca^{2+} (Supplementary Fig. 2) in the upper portion of the aquifer suggests that microbial aerobic methane oxidation is generating CO_2 , thereby leading to carbonic acid formation and acid-soluble (for example, carbonate) mineral dissolution. On the basis of previous CO_2 experiments³¹, carbonic acid-induced groundwater acidification may explain the increase in trace metals via dissolution and/or ion exchange processes. Although trace metals did not exceed drinking water limits over our monitoring period, these increasing trends may be of more significant concern given expected lifespans of shale gas wells¹⁴ or aquifers with different mineralogy. Given that the Borden sand is relatively inert (comprised primarily of quartz)²², groundwater

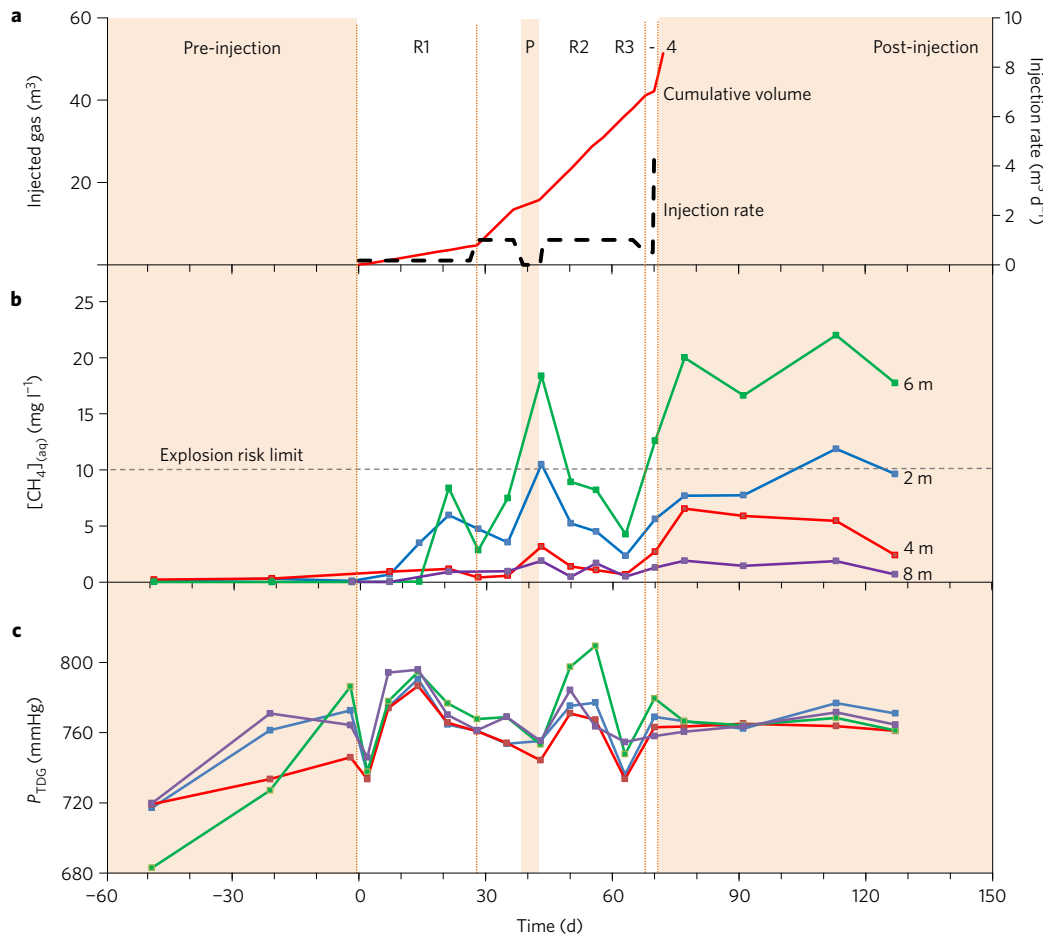


Figure 2 | Aqueous methane $[\text{CH}_4]_{\text{(aq)}}$ concentrations and total dissolved gas pressure (P_{TDG}) of the groundwater during methane injection and recovery periods. **a**, Experimental timeline showing the pre-injection period (−49 to 0 days), the injection rates employed (R1–R4) including cumulative volume of methane injected (0 to 72 days) and the post-injection period (72 to 150 days). **b,c**, Average $[\text{CH}_4]_{\text{(aq)}}$ (**b**) and P_{TDG} (**c**) with depth around the injection zone (that is, samples from points M2, M5, M6 and M7; Fig. 1c and Methods). $[\text{CH}_4]_{\text{(aq)}}$ and P_{TDG} evolve in a staggered manner with pressure increases preceding elevated $[\text{CH}_4]_{\text{(aq)}}$. Loss of gas injection pressure induced depth-discrete increases in $[\text{CH}_4]_{\text{(aq)}}$.

quality impacts in this experiment will be relatively low compared with aquifers containing more reactive minerals.

Methane gas efflux was detected at ground surface within hours of starting the injection. An equally rapid cessation of surface effluxes was observed when injection was stopped. The surficial CH_4 emission area was dependent on the injection rate and resulted in a ‘hotspot’ offset 1 m from the injection point (Fig. 3a). Continuous long-term chambers (LTCs) captured a high degree of temporal variability in surficial gas effluxes (Fig. 3b). Peak methane efflux rates at the three LTCs also varied spatially, even though the measurements were taken only 1 to 2 m apart (Supplementary Fig. 5). A conservative estimate based on the integration of all methane efflux rates over the experimental time suggests that at least 30% of the injected methane was emitted into the atmosphere (Supplementary Table 3); an additional portion was probably emitted as CO_2 after CH_4 oxidation in the vadose zone. Substantial ^{13}C enrichment of gas-phase methane in the vadose zone resulting in $\delta^{13}\text{C}$ values as high as −20 to −15‰ provides strong evidence for microbially mediated methane oxidation.

GPR measurements show that methane gas preferentially accumulated within a sequence of horizontally layered and interconnected sand lenses (Supplementary Fig. 6). The maximum GPR response occurred on day 65 (Fig. 4), where despite limited heterogeneity in the aquifer, methane migrated much faster and farther than that predicted by advective groundwater flow. This period of maximum lateral extent was accompanied by a

systematic decline in $[\text{CH}_4]_{\text{(aq)}}$ and P_{TDG} around the injection zone (Fig. 2b,c); here, rapid lateral expansion of free-phase gas in the direction of groundwater flow aided by horizontal bedding led to a temporary reduction in gas pressure and displacement of CH_4 -charged groundwater around the injection. These combined observations suggest that vertical buoyancy-driven methane gas migration and/or dissolution into groundwater over a period of days to weeks may influence the lateral extent of free-gas migration; however, the time and distance scales will depend on site-specific gas leakage rates and subtle variations in aquifer properties. In the case of our shallow unconfined aquifer, known to be relatively homogeneous in the context of single-phase fluid flow, fugitive free-phase methane spread more extensively than presupposed even for relatively low leakage rates and short time scales. Lateral migration will probably be more significant in deeper confined or partially confined aquifers subject to higher real-world leakage rates and stronger anisotropy in a multi-formational sedimentary sequence.

The potential for microbial attenuation of the released methane was investigated by screening the groundwater for methanotrophic bacteria with 16S ribosomal RNA gene amplicon sequencing. Prior to methane injection, methanotrophic microorganisms (for example, Methylococcaceae) were not detected. Methylotrophic microorganisms, which degrade one-carbon compounds but cannot oxidize methane (for example, Methylophilaceae), constituted <2% of the overall community and decreased in abundance with depth (Fig. 5a). Methane release strongly altered the microbial community

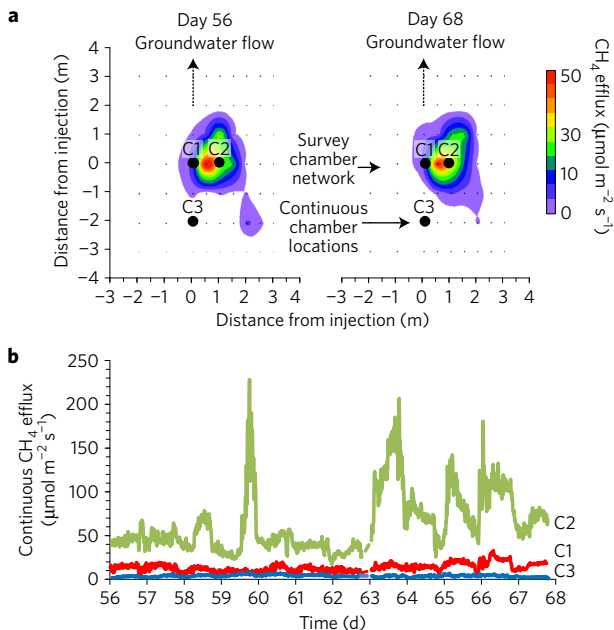


Figure 3 | Measured methane efflux to atmosphere during injection.

a, Spatial distribution of methane efflux on days 56 and 68 of the experiment. **b**, Continuous methane efflux measurements provided by the LTCs C1, C2 and C3 between days 56 and 68. Effluxes were episodic throughout the experiment despite constant injection rates during each injection phase. These spatiotemporal variations in efflux demonstrate the challenges associated with flux measurements and calculations, particularly those based on standard monitoring methods such as soil gas surveys, which have a much lower spatial resolution and are conducted only periodically.

structure (Fig. 5a) and stimulated growth of both aerobic methanotrophic Methylococcaceae and aerobic methylotrophic Methylophilaceae despite low oxygen concentrations throughout the aquifer (Supplementary Fig. 2). These two clades became very abundant at 2 and 4 m depth, with stable or increasing total cell numbers of up to 1.1×10^5 cells ml $^{-1}$ (Fig. 5b) indicating active populations. Their growth of the two clades also appeared to be coupled, as noted for oxygen-limited methane oxidation^{32,33}. An increase in the relative abundance of sulfate-reducing bacteria, related to Peptococcaceae, indicated that methane release led to anoxic conditions at 6 and 8 m, potentially a result of aerobic methane oxidation. This population shift was associated with a sharp decline in total cell counts at 6 m depth. Taxa capable of the anaerobic oxidation of methane were not detected, which, together with oxygen limitation, explains why microbial methane oxidation was relatively ineffective (Supplementary Fig. 2). However, methane injection strongly and persistently disturbed indigenous microbial communities, with no sign of recovery after 253 days.

During injection, the $\delta^{13}\text{C}$ values of dissolved methane in groundwater rapidly converged towards the carbon isotope ratio of the injected methane ($-42\text{\textperthousand}$). After 245 days, the $\delta^{13}\text{C-CH}_4$ remained unchanged and showed little indication of microbial conversion in the saturated groundwater zone (Supplementary Fig. 3). Isotope ratios indicate that methane was not significantly degraded within our monitoring period; however, more significant degradation, and therefore, potential water quality changes are expected to occur over longer time scales and with varying leakage rates, sediment composition and/or redox conditions.

Synthesis

Although the rates and duration of methane injection ($0.17\text{--}4.32 \text{ m}^3 \text{ d}^{-1}$ over 72 days) were relatively conservative in

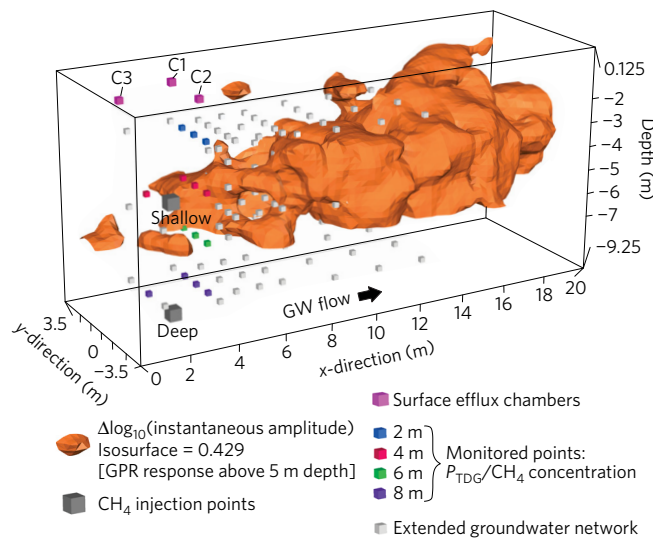


Figure 4 | GPR response associated with gas-phase methane accumulation extending downgradient from the injection points. The iso-surface boundary (orange zone) demarcates a laterally extensive volume of high-amplitude reflection events on day 65 (Methods and Supplementary Fig. 6), in the direction of groundwater flow impacted by methane gas accumulation beneath and along distinct sedimentary interfaces to a maximum sensing depth of 5 m below ground surface. Methane gas migrated >17 m downgradient, which is significantly greater than an estimate of ~ 6 m based on aquifer hydraulic properties and gradients²².

comparison with documented cases of leakage (Supplementary Information) and leakage scenarios deemed critical by regulatory agencies (that is, $>300 \text{ m}^3 \text{ d}^{-1}$)¹⁴, the lateral extent of the impacted groundwater zone relative to the depth of injection was substantial ($\sim 4:1$), significantly exceeding the observed methane emission footprint at surface. This large impact zone, as indicated by the GPR, was facilitated by small-scale geologic layering with subtly varying permeability, where the horizontal direction parallel to bedding represents the orientation of highest permeability. Here, the thin, finer, silty sand layers impeded upward migration of free gas, thereby trapping and shunting the gas laterally between coarser, more permeable interconnected sand layers, resulting in a hydrodynamically dispersed plume consisting of free-phase and dissolved methane (Fig. 6).

Free and dissolved-phase methane persisted in the groundwater throughout the 245-day monitoring period. Even a small mass of injected methane over a relatively short period of time ($\sim 36.4 \text{ kg}$ over 72 days) persisted due to lack of measurable microbial degradation in the aquifer volume investigated ($\sim 600 \text{ m}^3$); although, there was an appreciable perturbation to the indigenous microbial community in the groundwater zone. Hence, observed methane attenuation must for the most part be attributable to other processes; for example, efflux to the vadose zone during injection followed by advection, dispersion and diffusion.

On the basis of these observations, fugitive methane from a leaky petroleum well casing may have a strong propensity to migrate horizontally in deeper aquifers (Fig. 6). Here, anisotropy would facilitate lateral migration and retention of CH₄ in the groundwater zone, while buoyancy would enhance dispersion and upward migration to the vadose zone. The preferential mobility of free-phase gas along horizontal bedding planes will result in a laterally extensive and dispersed methane gas zone extending in the direction of groundwater flow, accompanied with hydrochemical alterations of groundwater. We show that both vertical and lateral gas migration mechanisms are important even when anisotropy is weak and the contribution of

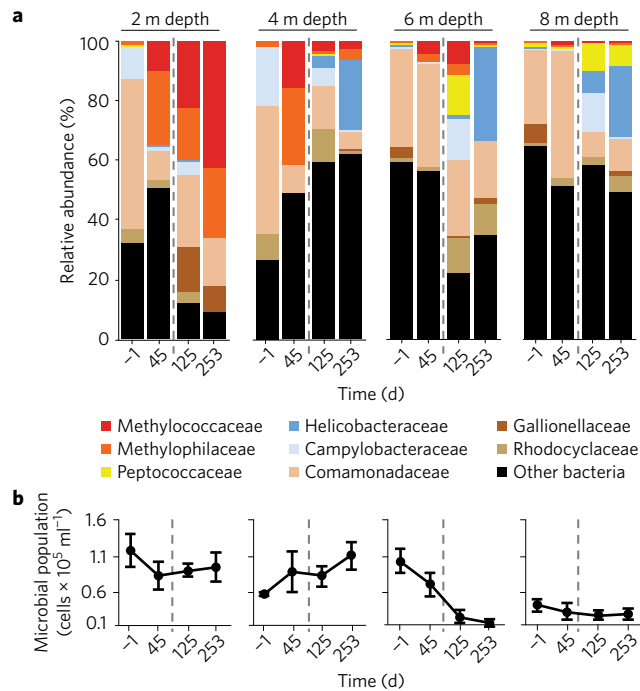


Figure 5 | Microbial response to injected methane gas in groundwater samples. **a**, Relative sequence abundances of bacterial taxa from monitoring well M6 (1 m downgradient of injection zone) determined by 16S rRNA gene amplicon sequencing. Methane was injected from day 0 to 72 (dashed line). Methanotrophs are shown in red, methylotrophs in orange, and sulfate reducers in yellow. Other taxa possibly involved in the cycling of sulfur and iron are shown in blue and brown, respectively. **b**, Total microbial cell counts at monitoring well M6 shown as average counts of ten independent microscopic fields; error bars are within two standard deviations of the mean.

each to groundwater flow will be site specific, depending primarily on anisotropy of the geologic medium. In bedrock units, fracture network conditions (aperture, orientation, length) will control the anisotropy and direction and magnitude of fluxes.

Regional groundwater flow systems

In sedimentary rocks, which are known to have very small effective porosities, advection of fluids is controlled by fractures and their connectivity. Therefore, for a given gas leakage rate, free gas will migrate much farther and faster in fractured sedimentary rock compared with a granular sand aquifer²¹ for a given specified gas injection (leakage) rate. Furthermore, the likelihood of leaks occurring deeper below multiple stratigraphic layers would be accompanied by stronger anisotropy, enhancing the rate of lateral migration parallel to bedding compared with upward migration orthogonal to bedding, but strongly influenced by the presence of long, through-going vertical pathways, possibly faults.

Current groundwater monitoring requirements in areas of energy resource development have perceived groundwater impacts to methane leakage as secondary to atmospheric emissions. However, our study shows that gas-phase migration from a high-pressure source in the saturated zone is an equivalent, if not, more significant process relative to atmospheric emissions. Present-day monitoring efforts do not consider the groundwater resource in its entirety and involve only periodic sampling from existing, sparsely located domestic wells, which serve as receptors at risk, rather than adequate monitors for groundwater resource impact evaluation. Current surface and subsurface monitoring efforts for shale gas development are thus insufficient to meaningfully detect or assess methane impacts to atmosphere and groundwater.

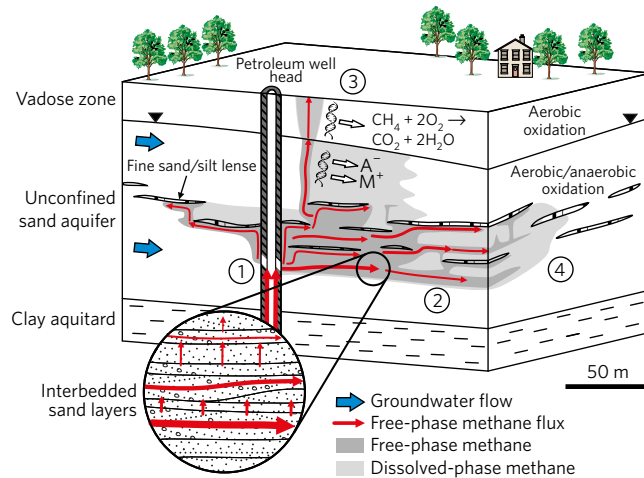


Figure 6 | Conceptual model of a continuous methane leak in an unconfined freshwater aquifer. (1) A compromised energy well casing releases methane; (2) laterally extensive free-phase gas migration controlled by subtle geologic variability; (3) variable methane efflux at the surface with potential for explosion risk and greenhouse gas emission; and (4) a temporally persistent dissolved methane plume. Aerobic oxidation of methane occurs in the vadose zone via microbes, but degradation is negligible in the saturated zone over 245 days. While vertical and lateral gas migration occurs simultaneously the relative magnitude of fluxes and style of resultant free-gas plume will depend on site-specific geologic conditions.

Our experimental field results show that subtle variations in aquifer properties can have a major impact on fugitive methane distribution, and that surface flux to the atmosphere is not indicative of the lateral extent of methane-induced groundwater quality impacts. Current efforts by oil and gas companies to locate and mitigate casing vent flow leaks or breaches in casings would identify entry points into the subsurface, and thus, facilitate groundwater impact monitoring strategies. Most importantly, we demonstrate that meaningful characterization and effective monitoring of fugitive methane in freshwater aquifers can be achieved through a multi-disciplinary and multi-scale monitoring network that intercepts and delineates a fugitive methane contaminant plume emanating from a leaky petroleum well.

Methods

Methods, including statements of data availability and any associated accession codes and references, are available in the online version of this paper.

Received 6 October 2016; accepted 20 February 2017;
published online 27 March 2017

References

- Malakoff, D. The gas surge. *Science* **344**, 1464–1467 (2014).
- Vidic, R. D., Brantley, S. L., Vandebossche, J. M., Yoxtheimer, D. & Abad, J. D. Impact of shale gas development on regional water quality. *Science* **340** (2013).
- Jackson, R. E. *et al.* Groundwater protection and unconventional gas extraction: the critical need for field-based hydrogeological research. *Ground Water* **51**, 488–510 (2013).
- Dusseault, M. B., Gray, M. N. & Nawrocki, P. A. *Why Oilwells Leak: Cement Behavior and Long-Term Consequences* (Society of Petroleum Engineers, 2000).
- Dusseault, M., Jackson, R. & MacDonald, D. *Towards a Road Map for Mitigating the Rates and Occurrences of Long-Term Wellbore Leakage* Special Report (Univ. Waterloo, 2014).
- Osborn, S. G., Vengosh, A., Warner, N. R. & Jackson, R. B. Methane contamination of drinking water accompanying gas-well drilling and hydraulic fracturing. *Proc. Natl Acad. Sci. USA* **108**, 8172–8176 (2011).

7. Darrah, T. H., Vengosh, A., Jackson, R. B., Warner, N. R. & Poreda, R. J. Noble gases identify the mechanisms of fugitive gas contamination in drinking-water wells overlying the Marcellus and Barnett Shales. *Proc. Natl Acad. Sci. USA* **111**, 14076–14081 (2014).
8. Heilweil, V. M. *et al.* Stream measurements locate thermogenic methane fluxes in groundwater discharge in an area of shale-gas development. *Environ. Sci. Technol.* **49**, 4057–4065 (2015).
9. Heilweil, V. M. *et al.* A stream-based methane monitoring approach for evaluating groundwater impacts associated with unconventional gas development. *Ground Water* **51**, 511–524 (2013).
10. Humez, P. B. *et al.* Occurrence and origin of methane in groundwater in Alberta (Canada): gas geochemical and isotopic approaches. *Sci. Total Environ.* **541**, 1253–1268 (2016).
11. Roy, N., Molson, J., Lemieux, J.-M., Van Stempvoort, A. & Nowamooz, A. Three-dimensional numerical simulations of methane gas migration from decommissioned hydrocarbon production wells into shallow aquifers. *Wat. Resour. Res.* **52**, 5598–5618 (2016).
12. *Shale Gas Extraction in the UK: A Review of Hydraulic Fracturing* DES2597 (The Royal Society, The Royal Academy of Engineering, 2012).
13. *Environmental Impacts of Shale Gas Extraction in Canada. The Expert Panel on Harnessing Science and Technology to Understand the Environmental Impacts of Shale Gas Extraction* (Council of Canadian Academies, 2014).
14. Nowamooz, A., Lemieux, J. M., Molson, J. & Therrien, R. Numerical investigation of methane and formation fluid leakage along the casing of a decommissioned shale gas well. *Wat. Resour. Res.* **51**, 4592–4622 (2015).
15. Ingraffea, A. R., Wells, M. T., Santoro, R. L. & Shonkoff, S.B. C. Assessment and risk analysis of casing and cement impairment in oil and gas wells in Pennsylvania, 2000–2012. *Proc. Natl Acad. Sci. USA* **111**, 10955–10960 (2014).
16. Caulton, D. R. *et al.* Toward a better understanding and quantification of methane emissions from shale gas development. *Proc. Natl Acad. Sci. USA* **111**, 6237–6242 (2014).
17. Jackson, R. B. *et al.* Increased stray gas abundance in a subset of drinking water wells near Marcellus shale gas extraction. *Proc. Natl Acad. Sci. USA* **110**, 11250–11255 (2013).
18. Molofsky, L. J., Connor, J. A., Wylie, A. S., Wagner, T. & Farhat, S. K. Evaluation of methane sources in groundwater in northeastern Pennsylvania. *Ground Water* **51**, 333–349 (2013).
19. Jackson, R. E. & Heagle, D. J. Sampling domestic/farm wells for baseline groundwater quality and fugitive gas. *Hydrogeol. J.* **24**, 269–272 (2016).
20. Siegel, D. I., Azzolina, N. A., Smith, B. J., Perry, A. E. & Bothun, R. L. Methane concentrations in water wells unrelated to proximity to existing oil and gas wells in northeastern Pennsylvania. *Environ. Sci. Technol.* **49**, 4106–4112 (2015).
21. Parker, B. L., Cherry, J. A. & Chapman, S. W. Discrete fracture network approach for studying contamination in fractured rock. *AQUA Mundi* **3**, 101–116 (2012).
22. Cherry, J. A., Gillham, G. W., Anderson, E. G. & Johnson, P. E. Migration of contaminants in groundwater at a landfill: A case study: 2. Groundwater monitoring devices. *J. Hydrol.* **63**, 31–49 (1983).
23. Sudicky, E. A. & Illman, W. A. Lessons learned from a suite of CFB Borden experiments. *Ground Water* **49**, 630–648 (2011).
24. Tomlinson, D. W., Thomson, N. R., Johnson, R. L. & Redman, J. D. Air distribution in the Borden aquifer during *in situ* air sparging. *J. Contam. Hydrol.* **67**, 113–132 (2003).
25. Cahill, A. G., Marker, P. & Jakobsen, R. Hydrogeochemical and mineralogical effects of sustained CO₂ contamination in a shallow sandy aquifer: a field-scale controlled release experiment. *Wat. Resour. Res.* **50**, 1735–1755 (2014).
26. Manning, A. H., Kip Solomon, D. & Sheldon, A. L. Applications of a total dissolved gas pressure probe in ground water studies. *Ground Water* **41**, 440–448 (2003).
27. Eltschlag, K. K., Hawkins, J. W., Ehler, C. & Baldassare, F. *Technical Measures for the Investigation and Mitigation of Fugitive Methane Hazards in Areas of Coal Mining* (Office of Surface Mining Reclamation and Enforcement, 2001).
28. Thomson, N. R. & Johnson, R. L. Air distribution during *in situ* air sparging: an overview of mathematical modeling. *J. Hazar. Mater.* **72**, 265–282 (2000).
29. McCray, J. E. Mathematical modeling of air sparging for subsurface remediation: state of the art. *J. Hazards Mater.* **72**, 237–263 (2000).
30. Johnson, P. C., Das, A. & Bruce, C. Effect of flow rate changes and pulsing on the treatment of source zones by *in situ* air sparging. *Environ. Sci. Technol.* **33**, 1726–1731 (1999).
31. Cahill, A. G., Jakobsen, R., Mathiesen, T. B. & Jensen, C. K. Risks attributable to water quality changes in shallow potable aquifers from geologic carbon sequestration leakage into sediments of variable carbonate content. *Int. J. Greenhouse Gas Control.* **19**, 117–125 (2013).
32. Beck, D. A. C. *et al.* A metagenomic insight into freshwater methane-utilizing communities and evidence for cooperation between the *Methylococcaceae* and the *Methylophilaceae*. *PeerJ* **1**, e23 (2013).
33. Oshkin, I. Y. *et al.* Methane-fed microbial microcosms show differential community dynamics and pinpoint taxa involved in communal response. *ISME J.* **9**, 1119–1129 (2015).

Acknowledgements

We acknowledge funding from the Natural Sciences and Engineering Research Council of Canada (NSERC), Strategic Project Grant no. 463045-14. Additional support was provided by the AITF/Eyes High Postdoctoral Fellowship programme (S.E.R.), the Campus Alberta Innovation Chair Program (M.S.), the Canadian Foundation for Innovation (M.S.), the Alberta Small Equipment Grant Program (M.S.), NSERC Discovery Grant (M.S.) and a Banting Postdoctoral Fellowship (C.M.S.). Special thanks for field assistance are given to A. Haggman, B. Ladd, D. Klazinga, T. Cheung, A. Verdin, R. Ingleton and P. Johnson.

Author contributions

A.G.C., B.L.P. and J.A.C. conceived, designed, installed and oversaw the experiment. A.G.C., C.M.S., O.F., O.K. and S.E.R. collected and processed all field data. All authors interpreted the multi-disciplinary data sets. A.G.C., B.L.P., J.A.C. and C.M.S. generated the first draft of the manuscript before all authors contributed to refinement and finalization.

Additional information

Supplementary information is available in the online version of the paper. Reprints and permissions information is available online at www.nature.com/reprints. Publisher's note: Springer Nature remains neutral with regard to jurisdictional claims in published maps and institutional affiliations. Correspondence and requests for materials should be addressed to B.L.P.

Competing financial interests

The authors declare no competing financial interests.

Methods

Injection system configuration and methodology. The gas delivery system was composed of two, 45°-inclined sparging wells emplaced at 4.5 and 9 m depths (termed shallow and deep). Each sparging well was constructed using a 1 m length of porous polyethylene (PE) well screen (SCHUMASOIL) connected to a mass flow controller and two canisters (master and slave) of industrial-grade methane by PE tubing. Injection screens were installed using a Geoprobe (model 7822DT) direct push system, along a vertical plane perpendicular to groundwater flow. Borden sediment is not freestanding following use of a Geoprobe direct push tool; drilled holes collapse almost immediately following removal of drill rods. Angled injection wells were used to minimize migration of methane along the delivery tube whilst maximizing gas release into the aquifer. Injection wells were connected to a control unit containing two individual (shallow and deep) mass flow controllers (Red-y smart GSC-C9SA-BB26) controlled by associated software (Get Red-y, Vögtlin Instruments AG).

Gas injection was conducted in four phases at three rates as shown in Supplementary Table 1. Total gas volume injected during the experiment was 51,350 l of industrial grade methane (34.9 kg at 1.013 bar and 15 °C). Following injection, gas delivery wells were sealed by non-return valves to prevent immediate flow back.

Aqueous chemistry sampling. Groundwater samples were collected through 32 multilevel groundwater sampling systems (M1–M32) comprising a total of 112 depth-discrete sample points (Fig. 1b). Sampling systems were constructed using 6 mm (OD) PE tubing connected to 5 cm length, geotextile-covered slotted PE screens (Nitex monofilament screen cloth, 200 µm mesh), fixed at multiple depths to a single polyvinyl chloride (PVC) centre-stock. Multilevel systems were instrumented with either three screens (2, 5 and 8 m depths), four screens (2, 4, 6 and 8 m depths) or five screens (2, 3, 4, 5 and 6 m depths) depending on the location and proximity to the injection point. The groundwater monitoring network covered an area of approximately 72 m², spanning 10 m downgradient of the injection zone. Multilevels were installed using a Geoprobe (model 7822DT) direct push system at higher density around and immediately downgradient of the injection zone at required depths. A plan view of the groundwater multilevel network sample points is shown in Fig. 1b.

Physical chemistry parameters including electrical conductivity (accuracy 1 µS cm⁻¹), pH (accuracy 0.02) and total dissolved gas pressure (1 mmHg) were measured with a multi-parameter water-quality sonde and flow-through cell (Manta 2, Eureka Water Probes) using a peristaltic pump at constant, low flow rate (approximately 40 ml min⁻¹). Dissolved gas samples were collected by filling either biocide-treated pre-evacuated 125 ml glass vials or 40 ml VOA vials, submerged in a beaker and piercing or sealing with a septa cap, respectively (leaving no headspace). Samples were stored upside down at 4 °C and measured on a Bruker 450 Natural Gas Analyzer for dissolved hydrocarbons (C1–C3) and other dissolved gases within 7 days. Major and minor cation concentrations were determined following filtration (0.45 µm cellulose acetate filters) and acidification for cation samples (concentrated HNO₃) by ion chromatography or inductively coupled plasma-mass spectrometry (ICP-MS; PerkinElmer Elan 6100DRC). Accuracy of ICP-MS measurements is 5% with limits of detection (mmol l⁻¹) for parameters shown as follows: Al, 1.11; Ba, 0.14; Ca, 3.74; Fe, 0.89; K, 1.27; Mg, 0.82; Mn, 0.036; Na, 2.17; Si, 3.55; Sr, 0.03; and Zn, 0.15. Alkalinity was determined (by Gran titration) for selected samples.

Experimental field site. The experimental site was characterized hydro-geochemically prior to methane injection through a series of depth-discrete background samples (three sampling events over 4 months prior to methane injection). A historic construction waste landfill leachate plume exists at the base of the aquifer (that is, 8–9 m depth)³⁴ creating two distinct aqueous chemistries. The upper zone, from the water table down to approximately 6–7 m depth, features sub-oxic groundwater (that is, negative Eh with low to no dissolved O₂) with moderate total dissolved solids (250–450 mg l⁻¹) and electrical conductivity (400–600 µS cm⁻¹) in the Fe/Mn reduction stage of the redox sequence and which is not currently impacted by landfill leachate. At 8 m depth, landfill leachate impacts the groundwater chemistry as evidenced by a significant increase in total dissolved solids (1,100–1,500 mg l⁻¹) and electrical conductivity (1,800–2,000 µS cm⁻¹) caused primarily by increases in concentrations of major ions and alkalinity. Concentrations of dissolved methane are naturally low (0.02–0.2 mg l⁻¹), the methane is of biogenic origin ($\delta^{13}\text{C}$ -CH₄ as low as -80‰), and $\delta^{13}\text{C}$ -CH₄ values occasionally as high as -48‰ suggest some occurrence of methane oxidation in the aquifer. Total dissolved gas pressure (P_{TDG}) is variable across the site, ranging from 700 to 860 mmHg (standard deviation 40–50 mmHg). Mean aqueous chemical conditions from three background samples taken 50, 21 and 2 days prior to injection are shown in Supplementary Table 2. The water table at the experimental site was approximately 1 m below ground surface during the duration of the experiment, varying ±0.5 m from spring to autumn, respectively.

Geophysical data collection and data processing. Ground-penetrating radar (GPR) measurements were collected using a PulseEKKO 100 GPR system (Sensors & Software) equipped with 200 MHz bistatic antennas and a 1,000 V transmitter. Reflection profiles were acquired along a series of parallel 20-m-long lines spaced 0.5 m apart, and orientated parallel to groundwater flow direction; these lines were connected by orthogonal tie lines positioned at 0.5, 8.5, 12, 15 and 18 m downgradient (Fig. 1c). Radar traces were recorded using a spatial step size of 0.1 m with the antennas spaced 1 m apart and orientated perpendicular to the survey line direction. A 64-trace stack was used with a temporal sampling interval of 800 ps. Data were recorded using a manual trigger and measuring tapes.

Post-acquisition processing and visualization were performed using ReflexW (v.7) (Sandmeier Software). The processing flow consisted of a high-pass mean dewow filter to remove d.c. shifts on individual traces; zero-time corrections; a fixed gain function to compensate for attenuation; a bandpass frequency filter (25–75–250–325 MHz); a notch frequency filter (40–85–85–125 MHz) to suppress ringing (for example, near-surface efflux chambers and electrical wires); and a three-trace horizontal filter. The instantaneous amplitude, a complex trace attribute that removes the effects of wavelet polarity and phase³⁵, was calculated to more accurately measure changes in reflection strength through the injection period. Here, the instantaneous amplitude provided a measure of changes in the dielectric contrast along closely spaced bedding planes. The high dielectric constant of water ($\kappa = 81$) relative to mineral grains ($\kappa = 4–6$) and air/gas ($\kappa = 1$) (ref. 36) results in a high reflection coefficient at the interface between contrasting stratigraphic units. In this study, the vertical and lateral migration of free-phase methane within the sand aquifer will be impeded at interfaces demarcating subtle changes in capillary properties. Subsequent accumulation of methane gas along these capillary boundaries will lead to a reduction in water saturation just below the interface as gas displaces water; this gas will continue to desaturate the pore space until the capillary pressure exceeds the air-entry pressure of the overlying sediment, upon which the gas will pass through³⁷. Spatiotemporal GPR amplitude variations along sedimentary interfaces were used to assess gas accumulation along stratigraphic bedding planes (Supplementary Fig. 6).

The spatial distribution of energy (that is, instantaneous amplitude) was calculated over a 20 × 7 m area using the reflection profiles shown in Fig. 1c. A three-dimensional cube (20 × 7 × 6 m) of the instantaneous amplitude was computed using an inverse distance weighting method based on a uniformly discretized 0.25 (x, y, z) grid, assuming a fixed radar velocity of 0.06 m ns⁻¹ (ref. 24).

Surficial efflux monitoring methods. Continuous methane effluxes were monitored with long-term LI-COR chambers (LI-8100-104) connected to a LI-COR Multiplexer (LI-8150) (LI-COR), cavity ring down laser spectroscopy, and extended range, Ultraportable Greenhouse Gas Analyzer (UGGA) (Los Gatos Research). The spatial distribution of gas effluxes was measured with a portable LI-COR chamber (LI-8100-103) connected to the UGGA³⁸.

Flux measurements were completed by placing chambers on PVC collars (0.2 m ID) inserted into the soil prior to commencing injection. The portable chamber was used in a 5 × 6 m grid and three long-term chambers were placed directly above (Chamber 1) and offset by 1–2 m (Chambers 2 and 3) from the methane injection (Supplementary Fig. 4). All chamber measurements lasted 3 min and an automated cycle switched between chambers every 10 min. Effluxes were calculated and are reported for selected times in micromoles per square meter per second (LI-COR, 2015).

Stable carbon isotope ratio measurements. Multilevel soil gas monitoring wells were installed (Supplementary Fig. 4) for periodic collection of soil gas samples and subsequent stable carbon isotope ($\delta^{13}\text{C}$) ratio analyses of methane and CO₂. Ports were installed at depths of 10, 30 and 50 cm. Wells were constructed of 1/8" gas-impermeable tubing with mesh screens at the bottom and gas-tight fitting and septa at the top. Samples were collected with gas-tight syringes (Valco Instruments) and stored in pre-evacuated 12 ml vials (Labco). Gas samples for isotope analyses were transferred directly using a gas-tight syringe (CH₄ > 3,000 ppmv) or via a pre-concentration device (CH₄ < 3,000 ppmv) into a Thermo Scientific Trace GC Ultra where methane was isolated and subsequently quantitatively converted to CO₂ at 1,000 °C using a GC-Isolink. The CO₂ was subsequently introduced into a Thermo Finnigan MAT253 isotope ratio mass spectrometer via a Conflo IV system, and carbon isotope ratios of methane were determined in continuous flow mode. Carbon isotope ratios of methane are reported in the standard delta notation (‰) relative to VPDB (Vienna PeeDee Belemnite) with a precision of better than ±0.5‰. $\delta^{13}\text{C}$ values of CO₂ were determined with the same system with a precision of better than ±0.3‰.

Microbiological sample filtration. Groundwater from the Borden aquifer for DNA analyses was collected in 1 l Nalgene HDPE bottles, which were completely filled and shipped in iced coolers to the Energy Bioengineering and Geomicrobiology laboratories at the University of Calgary. On arrival (5–7 days

after sampling), a 250 ml aliquot of each sample was filtered through a 0.22 µm GTTP Isopore membrane filter (Merck Millipore) attached to a sterile 500 ml polysulfone bottle top filter holder (Nalgene). The supernatant was collected in sterile 250 ml Schott bottles and subsequently filtered through a 0.1 µm Supor-100 membrane filter (Pall). The filters were stored at -20 °C until DNA extraction.

Microbial cell numbers. Unfiltered groundwater (5 ml) was fixed with sterile formaldehyde (final concentration, 4% v/v) and filtered through a sterile 0.1 µm Merck Millipore VCTP membrane filter. Cell counts from well M6 were performed using a DAPI (4',6-diamidino-2-phenylindole) stain³⁹ and fluorescence microscopy. Direct cell counts were performed and averaged for 10 fields of view.

DNA isolation and quantification. The 0.22 and 0.1 µm filters from each sample were cut into thin strips with a sterile scalpel and transferred in duplicate into autoclaved 2 ml bead beating tubes. Each tube contained 0.5 g of 0.1 mm and 0.5 g of 2.5 mm zirconia–silica beads (BioSpec Products). High-molecular-weight DNA was extracted from each filter using an SDS–chloroform protocol as follows. First, 300 µl each of 0.1 M phosphate buffer (pH 8), 10% SDS lysis buffer (pH 8), and 24:1 chloroform/isoamyl alcohol solution were added in sequence to the tubes. The tubes were loaded onto a bead mill homogenizer (Bead Ruptor 24, Omni) for 45 s at speed setting 5.5. The tubes were centrifuged at 20,000g for 5 min and the supernatant was transferred to a sterile 1.5 ml microcentrifuge tube. Ammonium acetate (7 mol l⁻¹) was then added to achieve a final concentration of 2.5 M. The 1.5 ml tubes were inverted gently by hand for 10 s and centrifuged at 20,000g for 7 min. The supernatant was transferred into a new sterile 1.5 ml microcentrifuge tube to which 0.54 ml of 100% isopropanol was added, then stored at -20 °C overnight for DNA precipitation. DNA was pelleted by centrifugation at 4 °C for 30 min. The isopropanol was decanted off and the tubes dried inside a biosafety cabinet for up to 2 h. The DNA in each set of duplicate tubes was re-suspended and pooled by dissolving the pellet in 30 µl of sterile nuclease-free water. DNA quantification was performed with a Qubit 2.0 Fluorometer (Thermo Fischer Scientific). DNA samples were stored at -20 °C. The constitution of 10% SDS lysis buffer (100 ml) was as follows: 48 ml MilliQ water, 2 ml of 5 M sodium chloride, 50 ml Tris solution (pH 8), and 10 g SDS. With the exception of isopropanol and chloroform/isoamyl alcohol solution, all reagents were filter-sterilized with a 0.22 µm syringe filter.

DNA amplification and Illumina 16S rDNA amplicon sequencing. The V3–V4 region of 16S rDNA was amplified in a single-step PCR using a KAPA HiFi HotStart reaction kit and primers Pro341F/Pro805R targeting all prokaryotes⁴⁰ and including Illumina adapters (Illumina). The primers were complementary to standard Illumina forward and reverse primers. The reverse primer also contained a 6-bp indexing sequence. PCR reaction conditions for DNA amplification were as follows: initial denaturation at 95 °C for 3 min, followed by 32 cycles of 95 °C for 30 s, 55 °C for 45 s, and 72 °C for 60 s, followed by a final step of 72 °C for 5 min. The amplicon products of triplicate PCR reactions were pooled and purified using AMPure XP beads (Agencourt Bioscience). DNA amplicon libraries were prepared from purified DNA using a Nextera XT DNA Sample Prep Kit with Nextera XT Index Kit (Illumina) as per the manufacturer's instructions. PCR conditions were as follows: 95 °C for 3 min, followed by 10 cycles of 9 °C for 30 s, 5 °C for 45 s, and

72 °C for 60 s, and a final step of 72 °C for 5 min. PCR products were purified with AMPure XP beads and quantified with a Qubit 2.0 Fluorometer. Amplicon libraries were normalized to 2 nM, pooled in equal volumes, denatured in 0.2 N NaOH, and diluted with hybridization buffer according to Nextera XT protocol. Paired-end sequencing (300 × 300 bp) of libraries at 15 pM final concentration was performed on an Illumina MiSeq instrument using the manufacturer's reagents and according to the manufacturer's instructions.

Analyses of 16S rDNA amplicon data. Paired-end reads (300 × 300 bp) were merged with usearch (3) ('-fastq_mergepairs -fastqminovlen 100-fastqmaxdiffs 8-fastq_allowmergestagger -fastq_trunqual 3'), followed by trimming of primers with Mothur⁴¹ ('trim.seqs pdiffs=0') and read quality control with usearch ('-fastq_filter -fastq_trunclength 350 -fastq_maxee 1'). DerePLICATION, removal of singleton and/or chimeric reads, and clustering was done with the uparse pipeline based on 97% sequence identity^{42,43}. Taxonomic assignment was done with the RDP classifier implemented in Mothur with the SILVA training data set as the template (http://www.mothur.org/wiki/Taxonomy_outline). Our approach is available online at <http://ebg.ucalgary.ca/metaamp>.

Data availability. The authors declare that the data supporting the findings of this study are available within the article and its Supplementary Information. DNA sequence data are available in the NCBI database (<https://www.ncbi.nlm.nih.gov>) (SRA accession **SRP076566**, Bioproject accession: **PRJNA32558**).

References

34. MacFarlane, D. S., Cherry, J. A., Gillham, R. W. & Sudicky, E. A. Migration of contaminants in groundwater at a landfill: a case study: 1. Groundwater flow and plume delineation. *J. Hydrol.* **63**, 1–29 (1983).
35. Sheriff, R. E. & Geldart, L. P. *Exploration Seismology* (Cambridge Univ. Press, 1995).
36. Cassidy, N. J. *Ground Penetrating Radar: Theory and Applications* (ed. Jol, H. M.) 41–72 (Elsevier, 2009).
37. Thomson, N. R. & Johnson, R. L. Air distribution during *in situ* air sparging: an overview of mathematical modeling. *J. Hazards Mat.* **72**, 265–282 (2000).
38. Porter, K. G. & Feig, Y. S. The use of DAPI for identifying and counting aquatic microflora. *Limnol. Oceanogr.* **25**, 943–948 (1980).
39. Sihota, N. J., Mayer, K. U., Toso, M. A. & Atwater, J. F. Methane emissions and contaminant degradation rates at sites affected by accidental releases of denatured fuel-grade ethanol. *J. Contam. Hydrol.* **151**, 1–15 (2013).
40. Takahashi, S., Tomita, J., Nishioka, K., Hisada, T. & Nishijima, M. Development of a prokaryotic universal primer for simultaneous analysis of bacteria and archaea using next-generation sequencing. *PLoS ONE* **9**, e105592 (2014).
41. Schloss, P. D. *et al.* Introducing mothur: open-source, platform-independent, community-supported software for describing and comparing microbial communities. *Appl. Environ. Microbiol.* **75**, 7537–7541 (2009).
42. Edgar, R. C. Search and clustering orders of magnitude faster than BLAST. *Bioinformatics* **26**, 2460–2461 (2010).
43. Edgar, R. C. UPARSE: highly accurate OTU sequences from microbial amplicon reads. *Nat. Methods* **10**, 996–998 (2013).